Effect of Plasma Shape on Electron Heat Transport in the Presence of Extreme Temperature Gradients Variations in TCV

A. Pochelon, Y. Camenen, R. Behn, A. Bortolon, A. Bottino, S. Coda, B.P. Duval, E. Fable, T.P. Goodman, M.A. Henderson, A.N. Karpushov, J.-M. Moret, A. Mück, E. Nelson-Melby, L. Porte, O. Sauter, A. Scarabosio, G. Zhuang and the TCV Team 1),
F. Ryter 2)
1) Centre de Recherches en Physique des Plasmas CRPP EPFL
Association EURATOM-Confédération Suisse
CH-1015 Lausanne, EPFL, Switzerland
2) Max-Planck-Institut für Plasmaphysik, EURATOM-IPP Association, Garching, Germany

e-mail contact of main author: Antoine.Pochelon@epfl.ch

Abstract. Electron heat transport experiments are performed in L-mode plasmas at various plasma triangularities, using radially localised electron cyclotron (EC) heating to vary the normalised electron temperature gradient R/L_{Te} (where $1/L_{Te}= \nabla T_e/T_e$) and the electron temperature T_e over an unusually large range. Local gyro-fluid (GLF23) and global collisionless gyro-kinetic (LORB5) linear simulations allow the determination of the unstable micro-instabilities. Ion temperature gradient (ITG) and trapped electron (TE) modes are found unstable. TE modes are the most unstable modes, except at the lowest R/L_{Te} values where they are stabilised and where ITG modes dominate. The high $Z_{eff}T_e/T_i$ leads to a complete stabilisation of the electron temperature gradient (ETG) modes. Experimentally, a strong dependence of the electron heat diffusivity χ_e on T_e is observed. No such clear dependence of the heat diffusivity χ_e is observed on R/L_{Te} or R/L_{ne}, in contrast to results from GLF23 simulations. The plasma collisionality ν_{eff} is found to strongly reduce the electron heat transport, consistent with the stabilisation of TE modes while increasing ν_{eff} in the simulations. However, the variation of ν_{eff} with δ prevents us from establishing the dependence of χ_e on δ quantitatively. Operationally, at a fixed total EC power, off-axis power deposition led to the formation of electron internal transport barriers (eITB) at low triangularity, more easily than at higher triangularity. This suggests ways of facilitating (or hindering) access to eITBs using plasma shaping.

1. Introduction

Plasma shape is one of the fundamental parameters in a tokamak that strongly influences plasma properties and performance, placing also strong constraints on technological and construction choices in machine design. Increasing the elongation allows higher plasma current and also influences other operational limits, such as the pressure [1,2] and density limits [3]. The triangularity (and elongation too) has a strong influence on the stability of core, e.g. sawteeth [4], and edge plasma, in particular on H-mode pedestal and ELMs [5].

This paper addresses the issue of the role of plasma shape in the energy confinement, focusing on the role of triangularity on the *local* electron heat transport properties in electron temperature gradient variation experiments using localised electron cyclotron (EC) power deposition. *Global* confinement studies in Ohmic [6-8] and in central EC heated L-mode plasmas [9,10] showed the beneficial role of low or negative triangularity on the electron energy confinement time. This result stands in contrast with results of similar studies of the influence of triangularity on H-mode confinement, where the confinement time increases with plasma triangularity [5], owing to the contribution of the edge pedestal, and also drastically modifies the ELM stability [11]. It is thought that the use of L-mode plasmas should help minimise the influence of the edge features on global confinement, allowing a more direct study of the genuine effect of plasma shape on core local electron heat transport. A better understanding of transport dependence on plasma shape may also open ways of influencing the threshold or access to eITB regimes. Such studies have also been started with an H-mode edge, therefore also under strong influence of ELM activity [12,13].

The specificity of the present study [14-16] lies in 1) the comparatively large range of both *normalised electron temperature gradients* $R/L_{Te}=R\cdot\nabla T_e/T_e$ [17,18], and *electron temperatures* explored, by changing respectively the radial EC power distribution and the total EC heating power; 2) the study of the influence of plasma shaping, in particular the *triangularity* δ, which is varied from Dee- to inverse-Dee-shape. In addition a third parameter, the plasma *collisionality*, plays a non-negligible role. While the first two parameters are operationally controlled, the third parameter cannot always be controlled independently.

2. Description of the experiments

2.1. TCV and EC system used: The TCV tokamak ($R_o = 0.88$ m, $a < 0.255$ m, $B_T < 1.54$ T, $I_p < 1$ MA) has been designed to investigate the effects of plasma cross-section shaping. Plasma edge triangularity $-0.7 < \delta < 1$ and elongation $1 < \kappa < 2.8$ have been achieved [8]. The auxiliary heating relies on EC waves at the 2nd harmonic (X2) and 3rd harmonic (X3) frequencies. The X2 EC waves are produced at 82.7 GHz by six gyrotrons delivering a total nominal power of 3 MW and are coupled to the plasma from the low field side (LFS), using six launchers independently steerable during the discharge [19].

2.2 Plasma discharges and experimental conditions: The experiments are performed in a moderately elongated L-mode plasma, $\kappa = 1.6$, in limiter configuration. The electron transport has been studied at three plasma triangularities, $\delta = \pm 0.2, +0.4$, while the plasma current I_p and the toroidal magnetic field B_T are kept constant ($I_p = 220$ kA and $B_T = 1.44$ T), implying a variation of the safety factor q_{95} from 4.4 to 5.5 (δ=-0.2, +0.4 respectively). Cross-field electron heat transport is investigated by depositing up to 1.8 MW X2 EC power in the plasma to vary the normalised electron temperature gradient R/L_{Te} and by distributing the power onto two different radial locations: one "central", at a deposition radius of $\rho_1 = 0.35$, just outside the $q = 1$ surface $\rho_{q=1}$, and one far off-axis, that is at $\rho_2 = 0.7$. The normalised radius is defined as $\rho = \mathrm{sqrt}(V/V_{LCFS})$, where V and V_{LCFS} are the volumes delimited by the flux surface labelled by ρ and by the last closed flux surface, respectively.

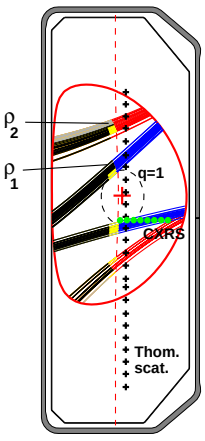

FIG. 1. ECH at two different deposition locations and line of sight of relevant diagnostics

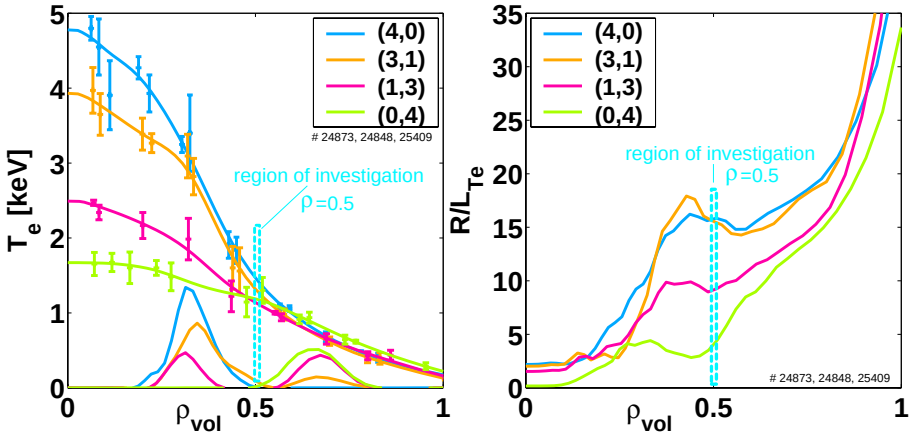

FIG. 2a. Electron temperature profile variations obtained at constant edge heat flux when changing the EC power deposition locations from central to off-axis.
FIG. 2b. Corresponding variations - up to a factor of 4 - of the normalised temperature gradient R/L_{Te}.

The central density range is fixed such as to avoid excessive refraction of the EC beams and to ensure full single pass absorption for the off-axis deposition ($1.5 < n_{eo} < 2.7\times10^{19}$ m^{-3}). The width of the EC beams, narrow compared to the plasma minor radius, leads to radially

localised EC power deposition. The EC power deposition width at half height $\Delta\rho_{EC}$ never exceeds 0.1 and the power absorption from the linear ray tracing code TORAY-GA [20], is above 95%. A poloidal view of the plasma cross-section and EC wave launch is shown in FIG. 1, for a case with simultaneous central and off-axis EC power deposition.

Thomson scattering, essential for this study, yields the electron temperature T_e and density n_e every 25 ms along the full plasma height with a spatial resolution of 4.5cm, typically 2×8 points in a full profile. Profile information is only used after steady state of the current profile is reached, that is stationary internal inductance l_i, and then averaged over 12 time slices (~ 300ms). Note that because of this procedure, the current profile shape (l_i) and ∇T_e are not independent variables.

2.3 Electron temperature profile and discharge response: Varying the amount of EC power deposited at ρ_1 from 0.45 to 1.8 MW does not change the shape of the T_e profile plotted in logarithmic scale, and R/L_{Te} only varies by 10% in the confinement region. This behaviour already observed in several tokamaks is known as profile resilience or stiffness [17]. To change the value of R/L_{Te}, off-axis distribution of part or total EC power is needed, e.g. following the scheme developed in ASDEX Upgrade to study electron heat transport as a function of the normalised electron temperature gradient [18]. Then, off-axis EC power deposition leads to low R/L_{Te} values whereas central deposition leads to high R/L_{Te} values. Intermediate R/L_{Te} values are achieved by sharing the deposited EC power centrally and off-axis. Keeping the total EC power constant, the variation of R/L_{Te} can be obtained at constant electron heat flux at the plasma edge, q_e^{edge}**,** without large changes of the electron temperature at the investigation radius, ρ=0.5. FIG. 2a shows the variation of the T_e profile, from peaked to flat, when changing gradually the EC power distribution from fully central to fully off-axis. This variation is obtained at constant edge T_e, as q_e^{edge} is kept constant. The corresponding R/L_{Te} profiles exhibit a variation by a factor of 4 in the region delimited by the two power deposition locations $\rho_1 < \rho < \rho_2$, typically at ρ=0.5, FIG. 2b. Varying the total EC power also allows covering a range of electron temperatures at constant R/L_{Te}.

In these experiments, cross-field electron heat transport is studied by calculating the electron thermal diffusivity χ_e defined by $q_e = -n_e \chi_e \nabla T_e$, from power balance. As a linear relation between the electron heat flux q_e and the electron temperature gradient ∇T_e is assumed, the effects of off-diagonal terms in the transport matrix are not included. The electron heat flux is calculated in steady-state taking into account the contributions of the Ohmic power, the localised EC power deposited at ρ_1 and ρ_2, the power transferred by the electrons to the ions and the temporal variation of the electron plasma energy. A radially uniform loop voltage is assumed in steady state for the calculation of the Ohmic power and the EC power is obtained from TORAY-GA. The ion temperature profile, needed to estimate the power transfer to the ions, is obtained from Charge Exchange Recombination Spectroscopy (CXRS, see FIG. 1). The power balance is strongly dominated by the EC power, which allows, by changing the EC power distribution, for a large variation of Q_e between ρ_1 and ρ_2, while keeping constant q_e^{edge}. The low plasma density and high T_e/T_i ratio results in a low equipartition power flow from electrons to ions. The radiated power P_{rad} measured by XUV-bolometer photodiodes never exceeds 20% of the total power P_{tot}. Moreover, the ratio P_{rad}/P_{tot} remains below 5% for ρ<0.8 and is therefore negligible in the region of investigation $\rho_1<\rho<\rho_2$.

The sawtooth activity present in these discharges confirms the expected deposition location just outside the q=1 surface $\rho_{q=1}$. The sawtooth period increases (sawtooth stabilisation) while increasing the power deposited at ρ_1, from 2-3ms in Ohmic to above 10ms with the total EC power. The observed sawtooth stabilisation indicates deposition just outside

$\rho_{q=1}$ [21,22], thus confirming TORAY ray tracing calculations. The sawteeth are of the "humpback" type, a combination of crashes and undulations, typically observed when heating off-axis, outside $\rho_{q=1}$ [23]. ASTRA transport calculations, using as inputs the experimental power balance heat conductivity χ_e^{PB}, the density and geometry, and assuming neoclassical conductivity and current profile steady-state conditions, allow retrieving the q-profile, without assumptions on a radial heat transport model [24]. The location of $\rho_{q=1}$ ranges from 0.28 to 0.34, FIG. 3, at the powers used, $\rho_{q=1}$ is always present. Since stationary conditions are required for diagnostics and transport analysis purposes, the imposed temperature profile variations produce asymptotic current profile changes (l_i is modified) [25]. The toroidal rotation velocity profile, measured form CXRS of C^{6+}-lines, is non-monotonic in Ohmic discharges [26], with a maximum close to $\rho_{q=1}$. A power deposition outside q=1, e.g. at mid-radius, peaks the central velocity profile and thus increases the velocity shear in the core.

3. Micro-instabilities (local transport: plasma parameters and codes)

Local gyro-fluid (GLF23 [27]) and global collisionless gyro-kinetic (LORB5 [28]) linear simulations indicate the unstable micro-instabilities possibly responsible for anomalous heat transport in these experiments. Ion temperature gradient (ITG) and trapped electron (TE) modes are found to be unstable. TCV data are depicted in the stability diagram, FIG. 4, which shows that TE modes are generally the most unstable modes, except at the lowest R/L_{Te} values where they are stabilised and where ITG modes dominate. The dashed lines indicate the pure TE threshold for a fluid model [29]. In all these EC dominated plasmas, the high values of $Z_{eff}T_e/T_i$, the quantity determining the electron temperature gradient (ETG) mode threshold [30], leaves the ETG modes stable (50% below threshold at mid-radius ρ=0.5).

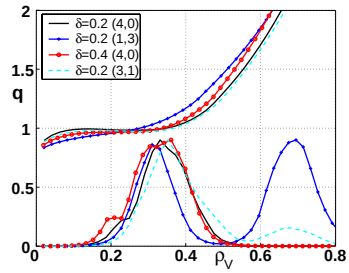

FIG. 3. q profiles from ASTRA with different EC power distribution (norm. to 0.9) and δ.

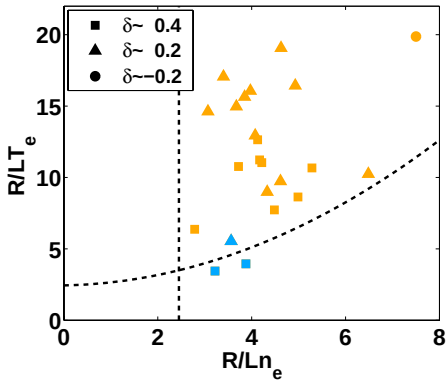

FIG. 4. Experimental values of the driving gradients for TE modes, R/L_{Te} and R/L_{ne}. From GLF23 simulations, TE modes dominate (in yellow), except for the lowest values of R/L_{Te}, where ITG modes dominate (in blue). The dashed lines indicate the pure TE threshold for a fluid model.

The ranges of the different relevant parameters at the investigation radius (ρ=0.53) for different power deposition distributions, total power and for two triangularities δ=0.2 and 0.4, is given in the following table (f_t: trapped particle fraction, ν_{eff}: collisionality [33], $s = \frac{r}{q}\frac{dq}{dr}$):

T_e [keV]	T_i [keV]	T_e/T_i	f_t	R/L_{Te}	R/L_{Ti}	R/L_{ne}	n_{e19} Z_{eff}	ν_{eff}	q	s
0.6–1.3	0.2–0.5	2-4	0.54–0.55	4-20	3.5-6.5	3-7.5	3.4-11.5	0.25-0.8	1.5-1-9	1.1-1.6

4. Inter-machine comparison within heuristic transport model

The "heuristic" model developed by Imbeaux and co-workers [31,32] predicts

$$\chi_e = \chi_0 + \lambda \cdot q \cdot T_e^{3/2} (R/L_{Te} - R/L_{Te}^{crit}) \cdot H (R/L_{Te} - R/L_{Te}^{crit}),$$

where q is the safety factor, λ and R/L_{Te}^{crit} are coefficients to be adjusted, H is the Heaviside function. To test the dependencies of this model against TCV data, the electron heat diffusivity in the gyro-Bohm normalised form is plotted against R/L_{Te} in FIG. 5a. ASDEX Upgrade data have been added for comparison. While the agreement with the model is

excellent for ASDEX Upgrade data, TCV data show a large scatter. The three different triangularities exhibit different levels of transport and scatter is found even at fixed triangularity. For $R/L_{Te} > 8$, the dependence of the normalised χ_e on R/L_{Te} is weak. The experimental T_e and R/L_{Te} ranges are shown in FIG. 5b. This broad two-dimensional range may be the cause of the larger spread of TCV data in FIG. 5a, implying that the dependences on $T_e^{3/2}$ or R/L_{Te} may not be entirely adequate. One additional effect could be a saturation of the diffusivity at high R/L_{Te}.

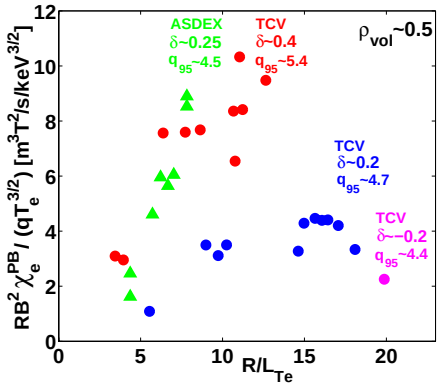

FIG. 5a. Inter-machine comparison of normalised heat conductivity (gyro-Bohm) versus normalised temperature gradient: ASDEX Upgrade (triangles), TCV at three different triangularities (circles)

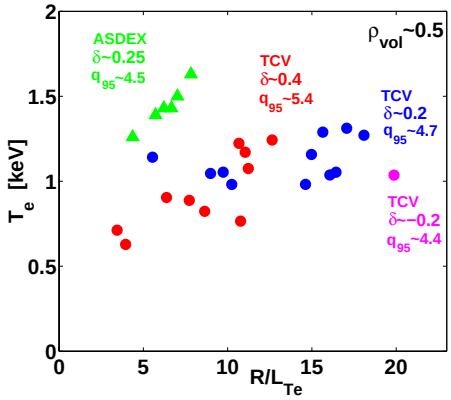

FIG. 5b. Range of data used in FIG 5a, showing that TCV data occupy a wide range in the T_e-R/L_{Te} space.

5. χ_e dependencies: experiment (and GLF23 simulations)

Concentrating momentarily on one triangularity δ=0.4 and depicting the heat diffusivities versus the driving terms of the TE modes (R/L_{Te}, R/L_{ne}) in FIG. 6a,b, we find that the variation of these two parameters is not sufficient to explain the variation of χ_e. Surprisingly, T_e alone appears to be a more adequate variable to reduce data scatter, FIG. 6c. The choice of the data at δ=0.4 to perform this test is suggested by the constancy of n_eZ_{eff} at this triangularity (see FIG. 9). Note that in FIG. 6c the two lowest χ_e points are not TE, but ITG mode dominated: these are also the two lowest points in FIG. 4, and seem to indicate the presence of a threshold in R/L_{Te}. The data above threshold yield a scaling with electron temperature as $\chi_e \sim T_e^{2\pm0.1}$.

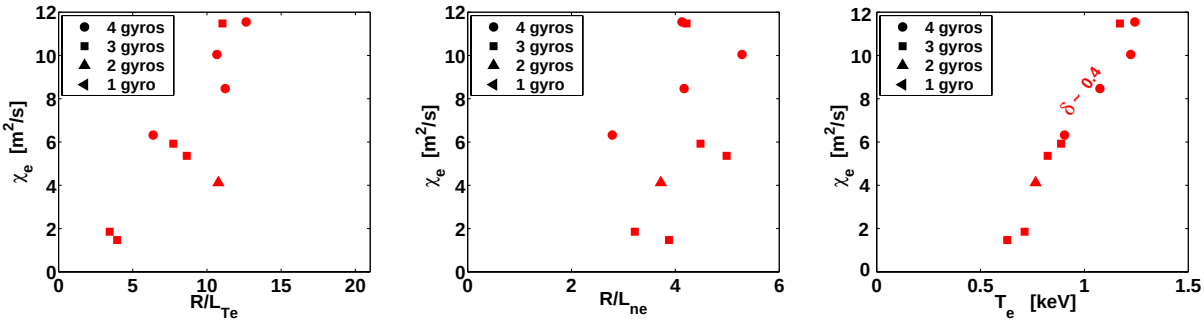

FIG. 6a,b,c. Checking the dependence of the electron heat diffusivity at δ=0.4 data against different variables at nearly constant n_eZ_{eff} (see FIG. 9). No clear dependence of χ_e is found on R/L_{Te}, FIG. 6a, or R/L_{ne}, FIG. 6b. A strong dependence on T_e, however, is observed, FIG. 6c.

This experimental observation of a strong χ_e-dependence on T_e does not exclude a weak dependence of χ_e on R/L_{Te} or R/L_{ne}, but is in contrast to the results from GLF23 simulations, which show a clear χ_e-dependence on R/L_{Te} or R/L_{ne}.

6. TCV data at different shapes and collisionalities

There are two forms of the heuristic critical gradient model for the heat flux q_e and diffusivity χ_e, which should be taken into account in the comparison with TCV data at high R/L_{Te}. The first form [31,32]:

$\chi_e \sim T_e^{3/2}(R/L_{Te}-R/L_{Te}^{crit})$, with a heat flux as $q_e \sim n_e T_e^{5/2}(R/L_{Te}-R/L_{Te}^{crit})R/L_{Te}$

or the more recent non-linear form in R/L_{Te}:

$\chi_e \sim T_e^{3/2}(R/L_{Te}-R/L_{Te}^{crit})/R/L_{Te}$, with a heat flux as $q_e \sim n_e T_e^{5/2}(R/L_{Te}-R/L_{Te}^{crit})$.

TCV data, for the diffusivities (FIG. 5a) as well as for the heat fluxes (FIG. 7a,b), are better represented by the second formulation. The heat fluxes at different triangularities follow a linear law as a function of R/L_{Te} or simply of ∇T_e. A low heat flux threshold above which the heat flux is enhanced is suggested from the diagram, **FIG. 7a,b**; The diffusivities rather show a saturation with R/L_{Te}. This representation clearly shows a beneficial effect of reducing triangularity on the extrapolated threshold (at q_e=0) for a given ∇T_e. Plotting χ_e versus T_e, for different triangularities, FIG. 8, shows in a clear way the beneficial role of reducing the triangularity (an extension of the diagram of FIG. 6c).

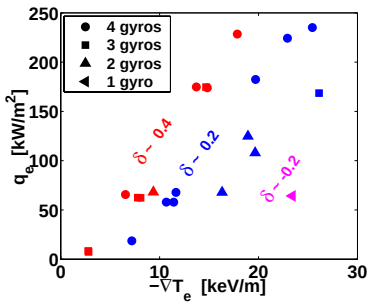

FIG. 7a. A large range of heat fluxes q_e and electron temperature gradients ∇T_e are explored at different triangularities. At constant heat flux, larger gradients are generated at lower triangularity.

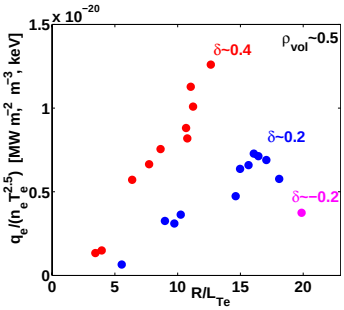

FIG. 7b. Test of the heat flux dependence on R/L_{Te}. It suggests a linear dependence of q_e on R/L_{Te} rather than a quadratic one.

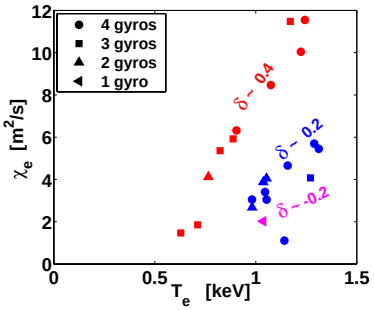

FIG. 8. Electron heat diffusivity versus electron temperature, showing a clear step-linear dependence for δ=0.4

The dependence on triangularity of the local electron heat transport parallels the global confinement time dependence in centrally heated discharges reported earlier [9,10]. This trend can further be illustrated in the present study with "central" (i.e. just outside $\rho_{q=1}$) and off-axis deposition by the confinement enhancement factor H_{98L}, FIG. 9, which increases when 1) the triangularity is reduced, and 2) the power is deposited the closest to the magnetic axis. FIG. 10 shows that the term $n_e Z_{eff}$ determining the collisionality ($\nu_{eff} \sim 0.1\ R n_e Z_{eff}/T_e^2$, see [33])

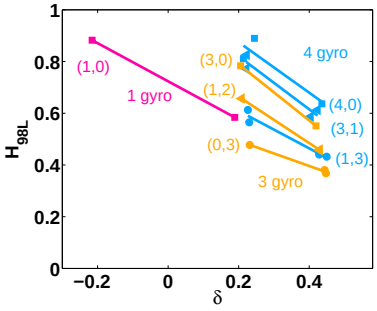

FIG. 9. Confinement enhancement factor for different deposition location and total power

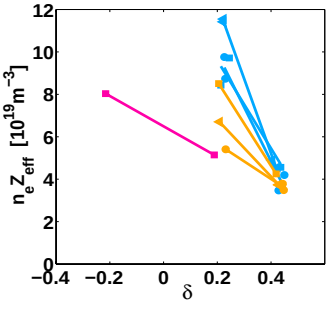

FIG. 10. Variation of $n_e Z_{eff}$ with triangularity.

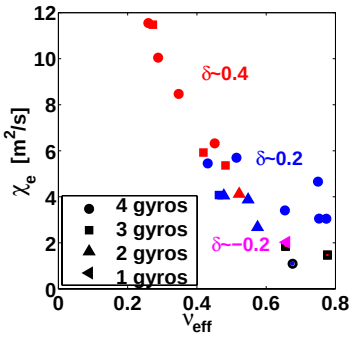

FIG. 11. Plasma collisionality ν_{eff} reduces strongly χ_e.

is nearly constant for all the δ=0.4 data, which were used to find the regression of FIG. 6c. Plotting all the χ_e data versus collisionality, FIG.11, reveals a possibly crucial role of collisionality in this transport study, where shape, heat deposition location and total heat flux are varied independently.

The electron heat transport is found to decrease strongly with plasma collisionality ν_{eff}, considered independently of shape and temperature, which is consistent with the stabilisation of TE modes while increasing ν_{eff} in GLF23 simulations. However, the strong data correlation of ν_{eff} with δ and temperature prevents us from establishing the dependence of χ_e on δ and ν_{eff} independently. To address the issue of the intrinsic effect of plasma shape, new experiments have recently been performed in which ν_{eff} is kept constant while δ is varied from –0.4 to 0.4 and will complement these results. Analysis of these data is under way.

Investigations of the influence of plasma shape on micro-instability-driven transport have been undertaken using the linear collisionless gyrokinetic code LORB5, to test TE mode stability and transport. For this purpose, experimental profiles measured at one triangularity, δ=0.2, have been kept constant while the triangularity was varied. The results demonstrate an effect of shape, triangularity, on the TE mode growth rate and transport. Growth rate and transport (estimated by mixing-length arguments) increase with both triangularity, in agreement with the experiment, FIG. 12, particularly in the toroidal mode number range $15<n<25$. FIG. 13a and 13b show that the spatial structure is also affected by the change of plasma shape.

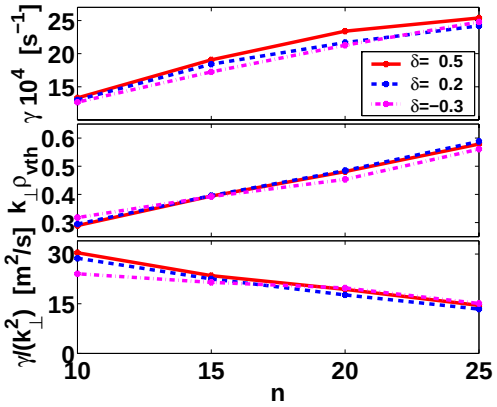

FIG. 12. TE mode growth rate γ, normalised radial extension, mixing length transport vs. toroidal mode number, showing the increase of transport quantities at high positive δ.

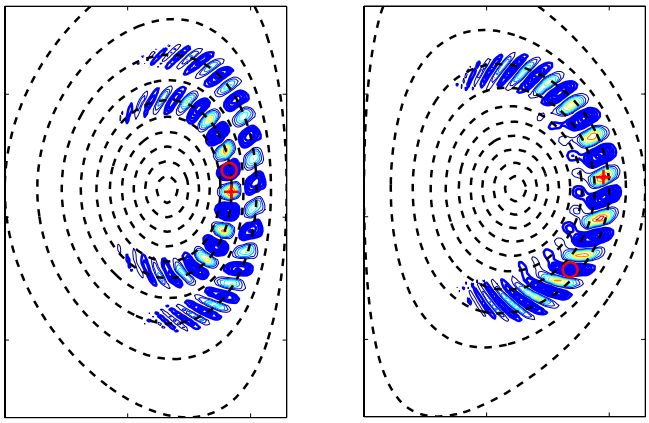

FIG. 13a,b. Poloidal cross-section of the electro-static potential for a TE mode at δ=-0.3 (a), and δ=0.5 (b). The spatial structure changes with triangularity.

7. Discussion and Conclusions

TCV experiments, with variations in both deposition distribution *and* total power, provide data along the two dimensions R/L_{Te} and T_e, an extension over experiments at constant total power in which R/L_{Te} and T_e remain correlated. The linear dependence of q_e on R/L_{Te} is very clear from the data and a saturation of χ_e with R/L_{Te} is strongly suggested, which compares well with recent simulations [34]. Note that such a saturation of χ_e with R/L_{Te} had been predicted by ITG modes simulations [35]. A clear dependence of χ_e on T_e is observed. At δ=0.4, TCV data can be explained by a weak or a vanishing dependence of χ_e on R/L_{Te} (and R/L_{ne}) well above the threshold and a strong dependence on T_e. The aim of this study was to find ways of improving/degrading confinement using plasma shape. χ_e is found to decrease with δ, as is also suggested from the linear collisionless gyrokinetic LORB5 results. However, the experimental search for the intrinsic dependence of electron heat transport on plasma

shape was made difficult by the variation of the collisionality with δ, through the quantity $n_e Z_{eff}$. The determination of the separate roles of shape and collisionality on transport requires triangularity scans at constant collisionality. Whether the dependence of $n_e Z_{eff}$ on triangularity is an issue of plasma-wall interaction or an issue of particle transport through the last closed surface, remains to be determined. It was indeed noticed that more gas injection is required in TCV to maintain the density constant in highly positive triangularity plasma, which in turn can explain the lower $n_e Z_{eff}$ by increased dilution. At the largest central power deposition, eITBs (large R/L_{Te}) have been obtained for the triangularity δ=0.2 (highest H_{98} in FIG. 9) and not for δ=0.4, which has a correspondingly higher χ_e. The present local transport investigations give some valuable indications on how to improve/hinder access to ITB by using triangularity variations.

This work was partially supported by the Swiss National Science Foundation.

Acknowledgements: The authors would like to acknowledge fruitful discussions with C. Angioni and L. Villard.

References

[1] TROYON, F. et al., Plasma Phys. Controlled Fusion **26**, (1984) 209.
[2] HOFMANN, F. et al., Phys. Rev. Lett. **81**, (1998) 2918.
[3] GREENWALD, M., et al. Nucl. Fusion **28** (1988) 2199.
[4] REIMERDES, H., POCHELON, A. et al., Plasma Phys. Contr. Fusion **42** (2000) 629.
[5] STOBER, J. et al., Plasma Phys. Control. Fusion **42** No 5A (May 2000) A211.
[6] WEISEN, H. et al., Nucl. Fusion **37** (1997) 1741.
[7] MORET, J-M., et al., Phys. Rev. Lett. **79** (1997) 2057.
[8] HOFMANN, F., et al., Plasma Physics and Controlled Fusion, **43** (2001) A161.
[9] POCHELON, A., GOODMAN,T.P., HENDERSON, M.A. et al., Nucl. Fusion **39**, No.11Y (1999) 1807.
[10] POCHELON, A., et al., Proc. of 26th EPS Conf. on Controlled Fusion and Plasma Physics, Maastricht, June1999, ECA Vol. **23J** (1999) 1089.
[11] BECOULET, M., HUYSMANS, G., SARAZIN, Y., et al., Plasma Phys. Controlled Fusion **45** (2003) A93.
[12] CRISANTI, F., LOMAS, P., TUDISCO, O. et al., Plasma Phys. and Controlled Fusion **45** (2003) 379.
[13] RIMINI, F.G., BECOULET, M., et al., this conference.
[14] CAMENEN, Y., POCHELON, A., et al. IAEA TM on ECRH, Klosterseeon, July 2003, Germany.
[15] POCHELON A., CAMENEN, Y., RYTER, F., CODA, S., EU-TTF Topical meeting on electron transport, February 19-20 2004, Milano, Italy.
[16] CAMENEN, Y., POCHELON, A., et al., 10th EU-US TTF Workshop, Sept. 6-9, 2004, Varenna, Italy.
[17] RYTER, F., et al., Plasma Phys. and Controlled Fusion **43** (2001) A323.
[18] RYTER, F., TARDINI, G. et al., Nucl. Fusion **43** (2003) 1396.
[19] GOODMAN T.P., ALBERTI. S., HENDERSON M.A., POCHELON A., TRAN M.Q., 19th Symp. on Fusion Technology, Lisbon, Portugal, 1996, Vol. **I** (1996) 565.
[20] MATSUDA, K., IEEE Trans. on Plasma Sci. **17** (1989) 6.
[21] ANGIONI, C., GOODMAN, T.P. et al., Nucl. Fusion **43** (2003) 455.
[22] MUECK A., et al., Proc. of 29th EPS Conf. on Controlled Fusion and Plasma Physics, Montreux, June 2002, ECA Vol. **26** (2002) P1-037 (http://epsppd.epfl.ch)., subm. for publ.
[23] PIETRZYK, Z.A., POCHELON, A., et al., Nucl. Fusion **39** (1999) 587.
[24] FABLE, E., SAUTER, O., Theory of Fusion Plasmas, 30 Aug. – 3 Sept. 2004, Varenna, Italy.
[25] POCHELON, A., ARNOUX, G., CAMENEN, Y., SCARABOSIO, A., ALBERTI, S., et al., 19th IAEA FEC, Lyon 2002, IAEA-CN-94/EX/P5-14.
[26] SCARABOSIO, A. et al., 46th Ann. Meeting of the Div. of Plasma Physics, APS, Savannah 2004.
[27] WALTZ, R.E., STEABLER, G.M., et al., Phys. of Plasmas **4** (1997) 2482.
[28] BOTTINO, A. et al., Phys. of Plasmas **11** (2004) 198.
[29] NORDMAN, H., WEILAND, J. et al., Nucl. Fusion **30** (1990) 983.
[30] JENKO, F., et al., Phys. of Plasmas **8** (2001) 4096.
[31] IMBEAUX, F., RYTER. F., GARBET, X., Plasma Phys. and Controlled Fusion **43** (2001) 1503.
[32] GARBET, X., et al., Plasma Phys. and Controlled Fusion **46** (2004) 1351.
[33] ANGIONI, C., et al., Physics of Plasmas **10** (2003) 3225.
[34] PEETERS, A., et al., subm. for publication, 2004.
[35] FIVAZ, M., EPFL Thesis 1692 (1997), Lausanne Report LRP 582/97.